GFZ
POTSDAM

Originally published as:

Wegmann, M. I., Riller, U., Hongn, F. D., Glodny, J., Oncken, O. (2008): Age and kinematics of ductile deformation in the Cerro Durazno area, NW Argentina:. - Journal of South American Earth Sciences, 26, 1, 78-90,

DOI: 10.1016/j.jsames.2007.12.004.

Age and kinematics of ductile deformation in the Cerro Durazno area, NW Argentina: significance for orogenic processes operating at the western margin of Gondwana during Ordovician – Silurian times

[published in: *Journal of South American Earth Sciences*, 2008;
doi: 10.1016/j.jsames.2007.12.004]

Maja I. Wegmann[1], Ulrich Riller[2], Fernando D. Hongn[3], Johannes Glodny[4], Onno Oncken[4]

[1] Freie Universität Berlin, Malteserstrasse 74-100, 12249 Berlin, Germany
[2] McMaster University, 1280 Main Street West, Hamilton, ON, L8S 4K1, Canada
[3] IBIGEO-CONICET, Universidad Nacional de Salta, Buenos Aires 177, 4400 Salta, Argentina
[4] GeoForschungsZentrum Potsdam, Telegrafenberg, 14473 Potsdam, Germany

Author for correspondence: Ulrich Riller
McMaster University
School of Geography and Earth Sciences
1280 Main Street West
Hamilton, Ontario
Canada, L8S 4K1

Phone: 905 525 9140 ext. 26365
Fax: 905 546 0463
E-Mail: rilleru@mcmaster.ca

Abstract

The Cerro Durazno Pluton belongs to a suite of Paleozoic granitoid intrusions in NW-Argentina, that are central for understanding the tectonic setting of the western margin of Gondwana in Ordovician and Silurian times. The pluton and its host rocks were tectonically overprinted by metamorphic mineral shape fabrics formed under middle greenschist-facies metamorphic conditions and associated with the nearby Agua Rosada Shear Zone. Kinematic analysis of the shear zone based on the geometric relationship between individual segments of the shear plane and principal axes of mineral fabric ellipsoids indicates reverse-sense of shear with a minor component of left-lateral displacement. This is compatible with the kinematics of other ductile deformation zones in this area, collectively forming a network, which accomplished orogen-parallel extension in addition to vertical thickening. Using the Rb-Sr isotopic system, an undeformed pegmatite dike of the Cerro Durazno Pluton was dated at 455.8 ± 3.6 Ma and mineral fabrics of the Agua Rosada Shear Zone formed at middle greenschist-facies metamorphism gave deformation ages of 437.0 ± 3.8 Ma and ≤ 428.4 ± 4.5 Ma. Thus, tectonic overprint at low metamorphic grade occurred about 20-30 Ma after terminal magmatism in the Cerro Durazno area. Our data from the Cerro Durazno area and regional considerations suggest that the western margin of Gondwana was characterized by orogen-parallel extension in addition to crustal thickening as well as episodes of magmatism and ductile deformation that varied greatly in time and space.

Key words: Gondwana, Paleozoic, ductile deformation, metamorphism, orogens, Argentina

Introduction

Knowledge of the temporal relationship between episodes of intrusion of Ordovician granitoid plutons and ductile deformation in NW-Argentina is critical for elucidating the geodynamic evolution of the western margin of Gondwana at that time. At the transition between the Puna and the Eastern Cordillera (Fig. 1), a prominent belt of Paleozoic granitoid plutons is exposed, whose genesis and tectonic significance has been the focus of many studies since its definition as the "Faja Eruptiva de la Puna Oriental" (Méndez et al., 1973). Multiple geodynamic scenarios have been proposed to account for the geodynamic setting of these plutons, which are part of the 300 km wide Ordovician magmatic belt that formed at the western margin of Gondwana.

The proposed scenarios include tectonic accretion of western Puna basement rocks either in Neoproterozoic to Early Paleozoic times (Bahlburg and Hervé, 1997) or during the Ordovician period (Ramos, 1999). Alternatively, basement rocks are regarded as Neoproterozoic to Early Paleozoic autochthonous lithotectonic units (Lucassen et al., 2000; Aceñolaza et al., 2000; Bock et al., 2000; Büttner et al., 2005). Models proposed for the formation of magmatic and metamorphic basement rocks located at the transition between the Puna and the Eastern Cordillera south of 24° S are equally diverse. These include the activity of (1) a magmatic arc that resulted from eastward subduction of oceanic crust below the western margin of Gondwana (Rapela et al., 1992), (2) an intracontinental magmatic belt located in the hinterland of such an arc in the western Puna (Coira et al., 1999; Zimmermann and Bahlburg, 2003), (3) an Early Paleozoic mobile belt that developed during a protracted thermal event related to a magmatic belt emplaced in autochthonous-parautochthonous basement rocks (Lucassen et al., 2000; Lucassen and Becchio, 2003; Viramonte et al., 2007), and (4) a non-collisional tectonic setting (Büttner et al., 2005), which may have been akin to that of the modern Andes in the same area (Lucassen and Franz, 2005; Hongn and Riller, 2007).

Paleozoic rocks of the eastern Puna and adjacent Eastern Cordillera include sinuous, dominantly N-S and NW-SE trending deformation belts (Fig. 1b). However, ages and kinematics of deformation as well as metamorphic conditions under which these belts

formed, are not well known yet (Le Corre and Rossello, 1994; Hongn et al., 1996, 1999; Hongn and Becchio, 1999). Late Neoproterozoic to Early Cambrian turbiditic sandstones of the Puncoviscana Formation (Turner, 1960) were tightly folded and affected by low-grade metamorphism in Early Cambrian time (Aceñolaza et al., 2000). During Cambrian to Silurian times, these rocks were transformed into phyllites, schists, gneisses and migmatites under regional metamorphic conditions (Rossi et al., 1992; Becchio et al., 1999; Lucassen et al., 2000; Büttner et al., 2005). Thus, the western margin of Gondwana seems to have been affected by a long period of medium-grade to high-temperature metamorphism (Lucassen and Becchio, 2003). Deformation appears to have been accomplished chiefly by regionally linked ductile deformation zones in Ordovician times (Hongn et al., 1996; Coira et al., 1999; Hongn and Mon, 1999).

South of 24° S, high-temperature metamorphic rocks are well exposed and host large masses of granitoid rocks (Figs. 1, 2), the vestiges of syn-orogenic magmatism (e.g., Méndez et al., 1973; Bahlburg, 1990; Lork and Bahlburg, 1993; Hongn, 1994; Omarini et al., 1999; Coira et al., 1999; Hongn and Riller, 2007). Here, ductile deformation zones such as the NW-SE striking Brealito and Agua Rosada Shear Zones merge with N-S striking zones forming a network of linked ductile deformation zones (Hongn and Mon, 1999). Emplacement of granitoid plutons occurred largely around 480 Ma to 470 Ma (Fig. 2). It is, however, uncertain to what extent individual deformation zones were active during granitoid magmatism and how much time elapsed between granitoid magmatism and ductile deformation at lower temperature metamorphic conditions.

The *circa* 480 Ma Cerro Durazno granite pluton (Haschke et al., 2005) intruded into high-temperature metamorphic rocks (Fig. 3). Hongn and Riller (2007) suggested that the pluton formed by emplacement of NE-SW striking, vertical magma sheets that coalesced into large magma bodies, under overall E-W shortening. The Agua Rosada Shear Zone (ARSZ: Hippertt and Hongn, 1998) formed at an advanced stage of pluton emplacement and at high-temperature metamorphism. This is indicated by the presence of granitoid dikes in the ARSZ, which are concordant to planar mineral fabrics formed at high temperature and interpreted as magma conduits during activity of the shear zone (Hongn and Riller, 2007).

Mineral fabrics formed under greenschist-facies metamorphic conditions and attributed to the ARSZ overprint magmatic mineral shape fabrics of the pluton. It is, however, uncertain whether the ARSZ was active during cooling from high-temperature to greenschist-metamorphic conditions or whether activity of the ARSZ ceased between the two metamorphic episodes evident by the mineral fabrics.

Therefore, a combined structural and geochronological study of the pluton and its low-temperature ductile overprint was aimed at unraveling the temporal relationship between the two. Using the geometry and orientation of metamorphic mineral shape fabrics observed at a total of 300 stations, the kinematics of the ARSZ is inferred. This is complemented by dating a pegmatite dike, indicating terminal magmatism, and metamorphic mineral shape fabrics of the ARSZ applying the Rb-Sr method.

General characteristics of the Cerro Durazno Pluton and its host rocks

The Cerro Durazno pluton and its metamorphic host rocks were affected by N-S-striking Cretaceous normal faults that were reactivated as reverse faults during Cenozoic Andean tectonism (Hongn and Seggiaro, 2001). N-S striking faults horizontally displaced the ARSZ, the granite - host rock contacts and NW-SE striking lithologic contacts of metamorphic host rocks, which are subparallel to the ARSZ at surface (Hongn and Riller, 2007, fig. 2).

Host rocks to the pluton vary in metamorphic grade and represent likely metamorphosed turbidites of the Puncoviscana Formation (Aceñolaza et al., 1976; Büttner et al., 2005). Northeast of the pluton (Fig. 3), a pervasive very low- to low-grade metamorphic transformation of pelite into schist is marked by the presence of chlorite and fine-grained muscovite defining cleavage planes. Toward the south, these rocks were affected by higher-grade metamorphism evident, in phyllite and schist, by chlorite and biotite porphyroblasts, and also by an increase in grain size towards higher-grade metamorphic rocks such as cordierite-bearing schist. Overall, there is a progressive increase in metamorphic grade from very low to high from NE to SW, i.e., toward the pluton, evident by the lithological

zonation (Fig. 3). However, high-temperature metamorphism in the Cerro Durazno area does not seem to be a local effect of pluton emplacement as high-temperature metamorphic rocks south of 25°S are spatially not restricted to pluton contacts (Fig. 1).

The Cerro Durazno pluton is composed of pink, coarse-grained, equigranular to porphyric granite. K-feldspar forms up to 4 cm long phenocrysts contained in a matrix of quartz, K-feldspar, plagioclase (ca. 30%), biotite (ca. 15 %) and subordinate muscovite. At the southern pluton margin, granitic magma intruded into migmatite (Fig. 3). Where possible to observe in the field, this contact is sub-vertical and lobate in map view. By contrast, the northeastern border of the pluton is rather straight, at the Earth's surface, and dips moderately toward the southwest. Along with a border-parallel foliation in both, the pluton and its host rock, in the border zone, the granite is affected by ductile deformation of the ARSZ. There, juxtaposition of granite against phyllite and schist as well as ductile deformation affecting also a 300 m wide granite dike within the ARSZ attest to the tectonic nature of the northeastern border (Fig. 3).

The pluton contains abundant microgranitoid enclaves and fragments of metamorphic host rock. Host rock fragments are mostly found at the pluton margin and display variable degrees of assimilation by the granite magma (Hongn and Riller, 2007). Pegmatite dikes are also common in the Cerro Durazno pluton and its host rocks. With a few exceptions, the dikes are deformed, characterized by planar margins and are concordant or at low angles to NW-SE striking zones of ductile deformation and metamorphic foliation in both pluton and host rocks.

The Agua Rosada Shear Zone

The ARSZ is an up to 500 m wide high-strain zone that developed chiefly in schist, migmatite and a NW-SE trending granite dike at the northeastern pluton margin (Fig. 3). Mineral shape fabrics of the ARSZ are characterized by foliation surfaces and mineral lineations that are inclined uniformly at angles between 60° and 80° toward the W (Fig. 4e). Oriented growth of fibrolite and biotite, elongate polymineralic aggregates, stretched

cordierite porphyroblasts and associated pressure shadows delineate the direction of maximum stretching in the ARSZ (Hongn and Riller, 2007). These minerals indicate that deformation proceeded under high-temperature metamorphic conditions.

Retrogression of cordierite into chlorite and muscovite as well as extensional fractures filled with quartz and feldspar suggest, however, that the ARSZ was also active during middle greenschist-facies metamorphism (Hongn and Riller, 2007). The main mineral phases in highly-strained granitoid rocks of the ARSZ are K-feldspar, plagioclase, white mica and quartz. Plagioclase and mica aggregates are of magmatic origin and form porphyroclasts enveloped by dynamically recrystallised quartz and fine-grained white mica, both displaying strong metamorphic layering. Quartz and white mica formed from transformation of K-feldspar, which occurs at low to middle greenschist-facies metamorphism (Kerrich et al., 1980; Fitz Gerald and Stünitz, 1993; Wintsch et al., 1995). Dynamic recrystallisation of quartz indicates temperatures above 300 °C during ductile deformation. In contrast to the matrix minerals, plagioclase porphyroclasts and mica aggregates show little evidence of dynamic recrystallisation suggesting that temperature during ductile deformation was below 450 °C (Fitz Gerald and Stünitz, 1993). Thus, strain fabrics of the ARSZ formed at high-temperature and lower temperature, i.e., greenschist-facies metamorphism.

The change from low- to high-temperature metamorphism toward the northeastern margin of the pluton is most conspicuous at the ARSZ (Fig. 3). Therefore, condensation of metamorphic isograds was accomplished likely by tectonic thinning linked to the development of the ARSZ. Tectonic condensation of metamorphic isograds by horizontal extension requires higher-grade rocks to be in the footwall of shear zones with normal sense-of-displacement. As migmatite and, by and large, micaschist are found, however, in the hanging wall of the southwest-dipping ARSZ, condensation of metamorphic isograds at the ARSZ is best explained by reverse sense-of-shear. The effect of tectonic thinning is obvious east of the N-S striking Cenozoic reverse fault where the migmatite almost disappears, thus placing the granite south of the ARSZ in contact with the quartzitic schists and phyllites immediately north of the shear zone (Fig. 3). This scenario may not preclude

condensation of isograds by horizontal extension preceding activity of the ARSZ. However, this would require the presence of northerly dipping planar strain fabrics, for which there is no evidence in the study area (Fig. 4).

Metamorphic mineral shape fabrics of the Cerro Durazno Pluton

Magmatic mineral shape fabrics can be discerned from metamorphic ones in the granite by their mineral assemblage and orientation. Magmatic fabrics are mostly planar and are defined by the shape-preferred orientation of biotite forming aggregates or individual crystals, or by euhedral K-feldspar phenocrysts (see also Hongn and Riller, 2007). At most localities, the magmatic foliation dips steeply toward the SE (Figs. 4a, b). Metamorphic fabrics transpose magmatic fabrics in the pluton and are characterized by planar (S) and linear (L) fabric geometry. Overall, planar components of L-S shape fabrics dip steeply toward the SW (Figs. 4a, c) and mineral lineations plunge dominantly toward the W (Figs. 4a, d).

Metamorphic mineral shape fabrics are defined by the shape-preferred orientation of the metamorphic assemblage chlorite + muscovite + quartz and indicate low-grade metamorphic conditions during deformation. Quartz is dynamically recrystallised, evident in thin section by its serrated grain boundaries, marginal formation of subgrains and undulatory extinction. Muscovite also underwent grain size reduction that is maximal in highly strained granitoid rocks. Relics of K-feldspar porphyroclasts displaying some undulatory extinction suggest, however, that solid-state deformation in these rocks began at temperatures exceeding 550 °C prior to deformation at low temperature (Hippertt and Hongn, 1998). Besides geometric similarity, ductile strain fabrics in the granite resemble to the fabrics of the ARSZ in the host rock in terms of metamorphism.

Metamorphic shape fabrics display variable intensities evident in the outcrop by the shape-preferred alignment of microgranitoid enclaves, biotite aggregates and K-feldspar phenocrysts as well as the spacing between quartz- and phyllosilicate-rich layers. Based on these observations, five levels of shape fabric intensity, O to IV, were defined (Figs. 3, 5):

Undeformed (intensity 0) granite is characterized by magmatic shape fabrics. Weakly deformed (intensity I) metagranite is delineated by the shape-preferred alignment of biotite aggregates and hypidiomorphic K-feldspar phenocrysts set in a coarse-grained matrix of quartz and plagioclase. Moderately deformed (intensity II) metagranite fabrics consist of biotite layers and elliptical K-feldspar augen. Mineral fabrics of strongly deformed (intensity III) rocks show a considerable reduction in grain size that affected chiefly K-feldspar, quartz and muscovite, collectively forming lenses or mm- to cm-wide layers. K-feldspar augen may display σ- or δ-type clast geometry. Grain size is at a minimum in mylonite and ultramylonite (intensity IV). These tectonites consist of thin laminae made of biotite, muscovite, chlorite and quartz hosting small plagioclase and K-feldspar porphyroclasts.

Shape fabric intensity was visually estimated and recorded at each station in the field. Weakly to moderately strained metagranite dominates the pluton center, whereas highly strained metagranite is dominantly found at the northeastern pluton margin. Shape fabric intensity is maximal in mylonite of the ARSZ (Fig. 3). In order to quantitatively calibrate the visual estimates of intensities I to III and to find out how fabric intensity relates to fabric geometry, the latter one was determined at selected sites in the field using the ellipticity of microgranitoid enclaves (Riller and Schwerdtner, 1997). More specifically, the ratio of the lengths of principal enclave axes $a > b > c$ was determined on sections approximating mineral layering (a-b plane), the plane perpendicular to the layering and parallel to the maximum mineral elongation (a-c plane) and, perpendicular to the maximum mineral elongation (b-c plane). Generally, the maximum and minimum diameters of about 15 enclaves were measured per section and their ratios averaged. Measurement of the ellipticity on two or more sections perpendicular to each other established that the shape ellipsoid for enclaves is truly tri-axial. Fabric intensity, i.e., departure from sphericity, was calibrated using d-values (Ramsay and Huber, 1983), the range of which for each level of visually estimated intensity is shown in the legend to Figure 3.

In granitoid rocks devoid of a tectonometamorphic overprint, the ratio between the length of the maximum and the minimum axis of enclaves may be up to 2.5. Thus, it is unlikely

that enclaves were perfectly spherical at the onset of post-emplacement ductile deformation of granitoid rocks. Therefore, our measurements of enclave ellipticity cannot be interpreted quantitatively in terms of accumulated strain resulting from the tectonic overprint. Enclave ellipticities of fabric intensities O to III are shown in a modified Flinn-diagram (Fig. 5). Evidently, shape fabric geometry becomes more oblate with increasing intensity, i.e., with increasing distance from the origin of the diagram. Such strain behaviour and overall increase in flattening strain and fabric intensity toward the ARSZ is typical for ductile shear zones (Ramsey and Graham, 1970; Coward and Potts, 1983). The width of this shear belt extends from the ARSZ to the southwest for a minimum of at least 2 kilometers into the Cerro Durazno Pluton (Fig. 4). The observed fabric elements of the shear belt are consistent with reverse shearing on the ARSZ forming the shear plane.

Kinematics of the Agua Rosada Shear Zone

Mylonites of the ARSZ contain abundant small-scale kinematic indicators such as S-C fabrics, σ- and δ- type porphyroclasts, asymmetric folds in the foliation and domains of preferred orientation of crystallographic quartz axes (Hippertt and Hongn, 1998; Hongn and Riller, 2007). However, the local sense of shear indicated by these structures is rather non-uniform. This is likely caused by the large flattening strains (Fig. 5) resulting in a significant departure from ideal simple shear geometry (S = L line in Figure 5). Overall flattening may well have been accomplished by non-coaxial deformation with variable shear strain directions on the scale of small-scale kinematic indicators. Thus, small-scale kinematic indicators cannot be used as reliable indicators for the overall sense-of-shear during low-temperature ductile deformation of the ARSZ.

Schwerdtner (1998) developed a simple graphical method, which determines the local sense of shear strain components using mineral shape fabrics as indicators of finite strain. The method can be applied to various tectonic settings, including transpressive deformation and oblique thrusting, and is particularly useful for determining the range of possible tangential shear strain vectors (γ), i.e., the sense-of-shear, of km-scale shear belts (Schwerdtner et al., 2005). The technique relies on the knowledge of the orientation of the shear plane or fault

zone, i.e., a lithotectonic boundary (LTB), and associated L-S mineral shape fabrics (Fig. 6). As these quantities are known from the ARSZ to some extent, application of this technique on metamorphic mineral fabrics associated with the ARSZ promises to indicate its sense of displacement based on finite strain.

It is generally possible to split the resultant shear strain vector into two oblique vectors γx and γz. The two vectors parallel, respectively, the orthogonal projection of the lineation direction (x) and the orthogonal projection of the foliation normal (z), onto the tangent plane to a high-strain-zone segment or its concordant fault ("LTB" in Figure 6a). The magnitude of the two vectors is generally unknown, but one may plot their directions on the upward facing side of the tangent plane to the high-strain zone (Fig. 6b). As pointed out by Schwerdtner (1998), the possible range of shear strain directions lies in the acute angle between γx and γz (Figs. 6b, c).

The orientation of the metamorphic mineral foliation (S) and lineation (L) is well known from the Cerro Durazno Pluton and the ARSZ (Fig. 4). By contrast, the exact orientation of the shear plane of the ARSZ, i.e., the LTB, is not accurately known. However, since the metamorphic mineral fabrics formed likely by ductile shear, the orientation of planar high-strain fabrics of the ARSZ may be chosen to represent the shear plane (Lin and Williams, 1992) and thus, may approximate the LTB at surface. Nonetheless, two fundamentally different kinematic scenarios are possible; (1) the shear plane is steeper than S and (2) the shear plane is shallower than S (LTB and LTB' respectively in Table 1).

In the first scenario, the mean values from all S-planes and mineral lineations measured in the Cerro Durazno area (Figs. 4c, d) are used to infer the orientation of principal strain axes $x > y > z$. The orientation for LTB is chosen to approximate that of planar high-strain fabrics of the ARSZ at surface (225/75: Fig. 7a). Projecting the x-axis, i.e., plunge of L, and the z-axis, through the LTB normal (LTBn) onto the LTB gives the possible range of shear strain vectors (about 70°) between the vectors γx and γz. A schematic vertical section through the xz principal plane of strain containing idealized traces of the LTB and of S-planes shows that this geometric relationship amounts to normal sense of displacement on

the LTB (Fig. 7b). Given the evidence for reverse sense-of-shear on the ARSZ presented beforehand, this kinematic scenario seems, however, unlikely.

For the second kinematic scenario, an orientation of the shear plane, LTB', is chosen that is shallower than S but has the same strike as LTB. The maximum possible inclination of LTB', for which projection of the x- and the z-axes results in reverse sense of displacement, as suggested by the condensation of metamorphic zones southwest of the ARSZ (Fig. 3), is indicated in Figures 7c and 7d. A small range of possible shear strain vectors plunging moderately westward between $\gamma x'$ and $\gamma z'$ is evident (Fig. 7c) and points to a component of left-lateral shear on the ARSZ. In this scenario, the shear plane dips less steeply than do high-stain fabrics at surface and it is likely that this geometric relationship applies to the ARSZ at depth. More specifically, the shear plane shallows with depth suggesting listric geometry of the ARSZ.

The tangential shear strain γ with its components γx and γz is related to the deflection from LTBn and can vary along the LTB. In order to assess the possible variation of shear strain direction with fabric intensity and locality within the ductile shear belt, the range of shear strain vectors was determined at five stations (Fig. 8, Table 1). In all graphical constructions, the orientation of LTB is kept constant, whereas the orientation of S and L varies according to their position in the field. As delineated beforehand, the maximum possible inclination of LTB', for which projection of the x- and the z-axes results in reverse sense of displacement, was chosen for each station. The progressive decrease in maximum dip of LTB' toward the southwest supports the notion that the ARSZ has listric geometry.

Except within the ARSZ, the angle between γx and γz is about 70° and thus, akin to the possible range of shear strain vectors of the first scenario. By contrast, the angle between $\gamma x'$ and $\gamma z'$ on LTB' is rather small, almost everywhere much less than 30°, and corresponds well with the range of shear strain vectors obtained from the second scenario. In summary, the possible range of shear directions does neither vary greatly with fabric intensity nor with position within the ductile shear belt. This indicates that the ARSZ formed by oblique reverse shear with a left-lateral shear component under overall E-W

shortening.

Ages of late-stage magmatism and low-temperature deformation

Felsic plutonic rocks in the eastern Puna were emplaced at an advanced stage of an apparently protracted high-temperature metamorphism between 515 Ma and 440 Ma (Becchio et al., 1999; Lucassen and Becchio, 2003). In order to constrain the time interval between waning granitoid magmatism of the Cerro Durazno Pluton and its tectonic overprint at greenschist-facies metamorphic conditions, both events were dated using the Rb-Sr system.

Terminal emplacement of granitoid magma of the Cerro Durazno Pluton is manifested by the presence of variably deformed pegmatite dikes. K-feldspar as well as 5 cm wide and up to 10 mm thick aggregates of white mica were taken from an unstrained dike (sample MW00-281: Fig. 3). Only white mica displaying non-deformed cleavage planes was used. Of these, transparent crystals were selected, from which inclusion-free portions were separated and washed with purified water and acetone. K-feldspar was separated from a homogeneous feldspar aggregate measuring about 50 cm^3.

To obtain the isotopic age of tectonic overprint at greenschist-facies metamorphism, two specimen of granitoid mylonite from the ARSZ were collected (samples MW00-151 and MW00-137b: Fig. 3). As delineated beforehand, the main mineral phases of ARSZ mylonite are K-feldspar and plagioclase enveloped by dynamically recrystallised quartz and fine-grained white mica, both displaying strong metamorphic layering. A requirement for dating deformation using the Rb-Sr isotope system is that the temperature during deformation remained below the closure temperature of the isotopic system in the mineral phase that formed during deformation (Villa, 1998). Based on the microstructure of ARSZ mylonite, the temperature at which ductile deformation occurred is estimated to have been between about 300°C and 450°C. As the Rb-Sr system in white mica closes at approximately 500 ± 50°C (Freeman et al., 1997), this system is well suited to date the tectonometamorphic overprint using recrystallised white mica in the ARSZ. More

specifically, the mineral age of recrystallised white mica forming the metamorphic layering is interpreted as the crystallization age during deformation at greenschist-facies metamorphic conditions, i.e., such mineral ages date the latest increments of progressive deformation of the specific sample (see detailed discussion in Freeman et al., 1997).

For the samples MW00-137b and MW00-151, syn-deformational, recrystallised feldspar and white mica was isolated from magmatic relics utilizing the distinct mineral grain size spectra. This was achieved by carefully breaking the samples by hand with a mortar, thereby avoiding crushing magmatic mica aggregates into smaller fractions. Recrystallized white mica as high Rb/Sr and K-feldspar as low Rb/Sr components were then separated using standard magnetic techniques, from the two samples. White mica was divided into sieve fractions (100-160 µm only for sample MW00-151; 160 - 250 µm, 250 - 355 µm, 355 - 500 µm) and K-feldspar crystals were separated into two grain-size fractions (< 160 µm and > 0.5 mm). For both, mica and feldspar, mineral concentrates of inclusion-free grains were generated by hand-picking under the binocular.

All samples were analysed applying the isotope dilution method to obtain the Rb and Sr contents. The samples were doped with a mixed ^{87}Rb-^{84}Sr spike solution and the silicates were dissolved with a mixture of HF and HNO_3. Rb and Sr were isolated using cation-exchange resin columns. Isotopic ratios were determined on a thermal ionisation mass spectrometer (VG Sector 54 multicollector TIMS, at GeoForschungsZentrum Potsdam). Details on Rb-Sr analytical procedures are given in Glodny et al. (2002). Standard errors, as derived from replicate analyses of spiked white mica samples, of ± 0.005% for $^{87}Sr/^{86}Sr$ ratios and of ± 1.5 % for Rb/Sr ratios were applied in isochron age calculations wherever individual analytical uncertainties were smaller than these values (cf. Kullerud, 1991). Isochron parameters were calculated using Isoplot/Ex 2.06 (Ludwig, 1999).

The Rb-Sr data are summarized in Table 2 and illustrated in Figure 9. The isochron age of the pegmatite sample MW00-281 is 455.8 ± 3.6 Ma (n = 5, MSWD = 1.4), calculated using all white mica and feldspar fractions (Fig. 9a). Integrity of isochron correlation between all mineral separates of different phases and grain sizes indicates that the age represents

pegmatite crystallization, from a Sr-isotopically homogeneous pegmatitic melt.

Rb-Sr analytical results of ARSZ mylonite samples were partly more complex than those of the pegmatite. Microstructural inspection of the mylonite showed that only very fine-grained white mica and K-feldspar entirely recrystallised during the latest stages of deformation. Nevertheless, for sample MW00-137b a valid Rb-Sr internal mineral isochron was obtained, corresponding to an age of 437.0 ± 3.8 Ma (n = 5, MSWD = 1.12; Fig. 9b). Differences in apparent ages between different mica grain size fractions cannot be resolved analytically for that sample.

In contrast, for sample MW00-151 the Rb-Sr analytical data scatter along a 436 ± 20 Ma reference line (MSWD = 7.2; Fig. 9c). Careful inspection of the data shows that there is a clear correlation between apparent white mica ages and mica grain sizes: While large white mica plots above the reference line, the smallest grain-size fractions tend to lower ages (Fig. 9c). There are two potential reasons for this data pattern. At one hand, the larger grain size fractions may include fragments of incompletely reset magmatic white mica, biasing our attempt to date greenschist facies deformation. On the other hand, the grain size vs. age correlation may result from protracted progressive dynamic recrystallization. It is well known that progressive deformation in mylonites causes grain size reduction, leaving 'large' white mica crystals as textural and isotopic relics from earlier stages of deformation (e.g., Müller et al. 1999). In both scenarios, the apparent age for the 'small' white mica grain size fractions (428.4 ± 4.5 Ma, including the 160 - 100 μm and 160 - 250 μm white mica combined with the data for K-feldspar < 160 μm; Fig. 9c) represents a maximum age for the end of ductile deformation in that sample. Considering the analytically indistinguishable apparent ages for the two smallest white mica fractions, the age value of 428 Ma most probably approximates very closely in time the last stage of ductile deformation.

Thus, the time interval between terminal magmatism of the Cerro Durazno Pluton at 455.8 ± 3.6 Ma and the end of the tectono-metamorphic overprint is about 20-30 Ma. The difference in deformation ages between the two mylonite samples suggests that greenschist-

facies ductile deformation along the ARSZ was a protracted process, lasting for a period of about 10 Ma. Protracted deformation during cooling is also consistent with the clear grain size vs apparent age correlation for white mica of the mylonite sample MW00-151.

Discussion

Granitoid plutons in the Eastern Puna and the Eastern Cordillera were emplaced between about 480 Ma and 440 Ma, i.e., at an advanced stage of an apparently long period of high-temperature regional metamorphism (515 Ma to 440 Ma: Becchio et al., 1999; Lucassen and Becchio, 2003). Magmatic activity in the Cerro Durazno area terminated with the emplacement of pegmatite dikes, for which we determined a Rb-Sr internal mineral isochron age of 455 Ma, at the waning stages of high-temperature metamorphism. Fabrics in the structural aureole of the Cerro Durazno Pluton corroborate that high-temperature metamorphism and regional deformation began before, and assisted in, the emplacement of the Cerro Durazno Pluton (Hongn and Riller, 2007).

The Rb – Sr isochron ages of 437 ± 3.8 Ma and ≤ 428 Ma for ARSZ mylonite suggest that ductile deformation at middle greenschist-facies metamorphism occurred about 20 - 30 Ma after emplacement of the Cerro Durazno Pluton. Although the ARSZ formed during pluton emplacement, planar magmatic fabrics in the pluton were not reoriented during development of L-S fabrics at greenschist-facies metamorphism of the ARSZ. This can be attributed to the heterogeneity of deformation that generated L-S fabric geometry. The strong discordance in the strike of both fabric types in the pluton may point to a lull in tectonic activity between formation of the two and thus, during cooling of the pluton and its host rocks. Pegmatite dikes and greenschist- to subgreenschist-facies metamorphism in the Sierra de Quilmes, located 25 km south of the Cerro Durazno Pluton (Fig. 2), were dated at 440 Ma and 416 Ma to 400 Ma, respectively (Büttner et al., 2005). The large difference in the ages of pegmatite dikes and deformation at low-temperature metamorphic conditions in both areas shows that pulses of terminal magmatism and ductile deformation are highly variable in space and time. Understanding the magmatic and metamorphic evolution on the orogen- scale thus requires structural and geochronological data from a larger area.

Geometrically and kinematically linked curvi-planar shear zones are a structural earmark of orogens that form by partitioning deformation in orogen-parallel extension and transverse shortening (Riller and Oncken, 2003; Cruden et al., 2006). The sinuous N-S and NW-SE striking shear zones of the eastern Puna (Fig. 1b), the ARSZ is part of, adhere well to such pattern of deformation zones. Kinematic analysis indicates that the ARSZ formed by E-W shortening, whereby a minor component of left-lateral ductile shear is also evident. Other shear zones in the eastern Puna, such as the Brealito Shear Zone (Fig. 1b: Hongn and Becchio, 1999; Hongn et al., 1999), a ductile fault next to the Cobres Pluton (Fig. 2: Hongn et al., 2006) and up to 300 m wide ductile shear zones in the Sierra de Quilmes (Fig. 2: Büttner et al., 2005), display similar kinematics. Collectively, these ductile shear zones postdate pluton emplacement and accomplished N-S extension in addition to vertical thickening. This rules out tectonic scenarios, by which the western Gondwana margin was affected by crustal thinning only during Ordovician and Silurian times (Büttner et al., 2005).

Components of left-lateral shear on NW-SE striking deformation zones, such as the ARSZ, can be explained by their obliquity with respect to the direction of orogen-parallel extension. Large, orogen-parallel transport of crustal entities as advocated by Aceñolaza et al. (2002) is, however, unlikely to have caused the rather small lateral shear component of the ARSZ or any of the aforementioned shear zones. In summary, any hypothesis accounting for the evolution of the western margin of Gondwana needs to include episodes of magmatism and deformation that may vary greatly in time and space and a tectonic setting controlled by orogen-parallel extension in addition to crustal thickening.

Conclusions

Our combined structural and geochronological study of the Cerro Durazno area, NW-Argentina, aids in understanding better the tectonic setting of the western margin of Gondwana in Ordovician and Silurian times. Analysis of the geometry, intensity and microstructure of metamorphic shape fabrics revealed that the Cerro Durazno Pluton was

tectonically overprinted by the Agua Rosada Shear Zone (ARSZ) under middle greenschist-facies metamorphic conditions. Results of our kinematic analysis attest to reverse-sense of tangential ductile shear in the ARSZ, with a minor left-lateral component. This is consistent with the kinematics of other shear zones in the eastern Puna and Eastern Cordillera suggesting overall N-S, orogen-parallel extension in addition to vertical thickening. Large, orogen-parallel transport of crustal entities is difficult to reconcile with any of the Paleozoic ductile shear zones in the eastern Puna and Eastern Cordillera.

An undeformed pegmatite dike of the Cerro Durazno Pluton was dated at 455.8 ± 3.6 Ma and mineral fabrics of the ARSZ formed under middle greenschist-facies metamorphic conditions were dated at 437.0 ± 3.8 Ma and ≤ 428.4 ± 4.5 Ma. Activity of the ARSZ may have paused between terminal magmatism and tectonic overprint in the Cerro Durazno area. Geochronological data from this area and the nearby Sierra de Quilmes suggest that magmatic and tectonic episodes varied greatly with time and position, a characteristic that needs to be considered in any tectonic setting accounting for the evolution of the western Gondwana margin.

Acknowledgment

This work was funded by the German Science Foundation as part of the Collaborative Research Program SFB 267 and the German Ministry of Development (BMZ). F. Hongn acknowledges supported from the ANPCyT (PICT 7-12417)-CIUNSa (1235). We thank W.M. Schwerdtner and two anonymous reviewers for scrutinizing the manuscript.

References

Aceñolaza, F.G., Durand, F., Diaz Taddei, R., 1976. Geología y contenido paleontológico del basamento de la región de Cachi, provincia de Salta, República Argentina. Actas VI Congreso Geológico Argentino 1, 319-332.

Aceñolaza, F.G., Miller, H., Toselli, A.J., 2000. The Pampean and Famatinian cycles – Superposed orogenic events in West Gondwana. In: Miller, H., Hervé, F. (Eds.), Geoscientific Cooperation with Latin America. Zeitschrift für Angewandte Geologie, Sonderheft SH1., 31st International Geological Congress, pp. 337-344.

Aceñolaza, F.G., Miller, H., Toselli, A.J., 2002. Proterozoic – Early Paleozoic evolution in western South America – a discussion. Tectonophysics 354, 121-137.

Bock, B., Bahlburg, G., Wörner, G., Zimmermann, U., 2000. Tracing crustal evolution in the southern Central Andes from Late Precambrian to Permian with geochemical and Nd and Pb isotopic data. Journal of Geology 108, 515-535.

Bahlburg, H., 1990. The Ordovician basin in the Puna of NW Argentina and N Chile: Geodynamic evolution from back-arc to foreland basin. Geotektonische Forschungen 75, 1-107.

Bahlburg, H., Herve, F., 1997. Geodynamic evolution and tectonostratigraphic terranes of northwestern Argentina and northern Chile. Geological Society of America Bulletin 109, 869-884.

Becchio, R., Lucassen, F., Kaseman, S., Franz, G., Viramonte, J., 1999. Geoquímica y sistemática isotópica de rocas metamórficas del Paleozoico inferior. Noroeste de Argentina y Norte de Chile (21°-27°S). In: Colombo, F., Queralt, I., Petrinovic, I. (Eds.), Geología de los Andes Centrales Meridionales: El Noroeste Argentino. Acta Geológica Hispánica 34, 273-299.

Büttner, S.H., Glodny, J., Lucassen, F., Wemmer, K., Erdmann, S., Handler, R., Franz, G., 2005. Ordovician metamorphism and plutonism in the Sierra de Quilmes metamorphic complex: Implications for the tectonic setting of the northern Sierras Pampeanas (NW-Argentina). Lithos 83, 143-181.

Coward, M.P., Potts, G.J., 1983. Complex strain patterns developed at the frontal and lateral tips to shear zones and thrust zones. Journal of Structural Geology 5, 383-399.

Coira, B., Kay, S., Pérez, B., Woll, B., Hanning, M., Flores, P., 1999. Magmatic sources and tectonic setting of Gondwana margin Ordovician magmas, northern Puna of Argentina and Chile. In: Ramos, V.A., Keppie, J. D. (Eds.), Laurentia-Gondwana Connections before Pangea. Boulder, Colorado, Geological Society of America Special Paper 336, pp.1-26.

Cruden, A., Nasseri, M.H.B., Pysklywec, R., 2006. Surface topography and internal strain variation in wide hot orogens from three-dimensional analogue and two-dimensional numerical vice models. In: Buiter, S.J.H., Schreurs, G. (Eds.), Analogue and numerical modelling of crustal-scale processes. Geological Society, London, Special Publications 253, pp. 79-104.

Fitz Gerald, J.D., Stünitz, H., 1993. Deformation of granitoids at low metamorphic grade, I. Reactions and grain size reduction. Tectonophysics 221, 269-297.

Freeman, S.A.R., Inger, S., Butler, R.W.H., Cliff, R.A., 1997. Dating deformation using Rb-Sr in white mica: Greenschist facies deformation ages from the Entrelor shear zone, Italian Alps. Tectonics 16, 57-76.

Flinn, D., 1962. On folding during three dimensional progressive deformation. Quarterly Journal of the Geological Society of London 118, 385-428.

García, H.H., Rossello, E.A., 1984. Geología y y yacimientos minerales de Papachacra, Depto. Belén, Catamarca, Argentina. Actas, IX Congreso Geologico Argentino, San Carlos de Bariloche 7, 245-259.

Glodny, J., Bingen, B., Austrheim, H., Molina, J.F., Rusin, A., 2002. Precise eclogitisation ages deduced from Rb/Sr mineral systematics: The Maksyutov complex, Southern Urals, Russia. Geochimica et Cosmochimica Acta 66(7), 1221-1235.

Haschke, M., Deeken, A., Insel, N., Sobel, E., Grove, M., Schmitt, A. 2005. Growth pattern of the Andean Puna plateau constrained by apatite (U/Th)/He, K-feldspar $^{40}Ar/^{39}Ar$, and zircon U-Pb geochronology. Proceedings, 6th International Symposium on Andean Geodynamics (ISAG 2005, Barcelona), 360-363.

Hippertt, J.F., Hongn, F.D., 1998. Deformation mechanisms in the mylonite/ultramylonite transition. Journal of Structural Geology 20, 1435-1448.

Hongn, F. D., 1994. Estructuras precámbricas y paleozoicas del basamento del borde oriental de la Puna; su aplicación para el análisis regional de la faja eruptiva. Revista de la Asociación Geológica Argentina 49, 256-268.

Hongn, F.D., Mon, R., Cuevas, J., Tubia, M., 1996. Zones de cisaillement caledoniennes a haute temperature dans la Quebrada Barranquilla (Puna orientale, Argentine): donnees structurales et cinematiques. C.R. Acad. Sci. Paris 323, serie IIa, 809-815.

Hongn, F. D., Mon, R., 1999. La deformación ordovícica en el borde oriental de la Puna. In: González Bonorino, G., Omarini, R., Viramonte, J.G. (Eds.), Geología del Noroeste Argentino. Relatorio 14º Congreso Geológico Argentino, Salta 1, pp. 212-216.

Hongn, F.D., Becchio, R.A., 1999. Las fajas miloníticas de Brealito, Valles Calchaquíes, Salta. Revista de la Asociación Geológica Argentina 54, 74-87.

Hongn, F., Aranguren, A., Tubía, J.M., Mon, R., 1999. Estructura, fábrica magnética y emplazamiento de los granitos de Brealito y La Paya, basamento del Valle Calchaquí, Salta, Argentina. In: Colombo, F., Queralt, I., Petrinovic, I. (Eds.), Geología de los Andes Centrales Meridionales: El Noroeste Argentino. Acta Geológica Hispánica 34(2-3), pp. 301-317.

Hongn, F. D., Seggiaro, R. E., 2001. Hoja Geológica 2566-III, Cachi, 1:250.000. SEGEMAR. Boletín 248. Buenos Aires.

Hongn, F., Mon, R., Acuña, P., Kirschbaum, A., Menegatti, N., 2006. Deformación intraordovícica en la sierra de Cobres. Asociación Geológica Argentina, Serie D: Publicación Especial Nº10, p. 186-192.

Hongn, F., Riller, U., 2007. Tectonic evolution of the western margin of Gondwana inferred from syntectonic emplacement of Paleozoic granitoid plutons in NW-Argentina. Journal of Geology 115, 163-180.

Kerrich, R., Allison, I., Barnett, A.L., Moss, S., Starkey, J., 1980. Microstructural and chemical transformations accompanying deformation of granite in a shear zone at Miéville, Switzerland; with implications for stress corrosion cracking and superplastic flow. Contributions to Mineralogy and Petrology 73, 221-242.

Kullerud, L., 1991. On the calculation of isochrons. Chemical Geology 87 (2), 115-124.

LeCorre, C.A., Rossello, E.A., 1994. Kinematics of early Paleozoic ductile deformation in the basement of NW-Argentina. Journal of South American Earth Sciences 4, 301-308.

Lin, S., Williams, P.F., 1992. The geometrical relationship between the stretching lineation and the movement direction of shear zones. Journal of Structural Geology 14 (4), 491-497.

Lork, A., Miller, H., Kramm, U., 1989. U-Pb zircon and monazite ages of la Angostura granite and the orogenic history of the northwestern Argentine basement. Journal of South American Earth Sciences 2, 147-153.

Lork, A., Bahlburg, H., 1993. Precise U-Pb Ages of Monazites from the Faja Eruptiva de la Puna Oriental and the Cordillera Oriental, NW Argentina. Actas XII Congreso Geológico Argentino y 2° Congreso de Exploración de Hidrocarburos, Mendoza 4, 1-6.

Méndez, V., Navarini, A., Plaza, D., Viera, V., 1973. Faja eruptiva de la Puna oriental. Actas V Congreso Geológico Argentino, Córdoba 4, 89-100.

Lucassen, F., Becchio, R. 2003. Timing of high-grade metamorphism: Early Paleozoic U-Pb formation ages of titanite indicate long-standing high-T conditions at the western margin of Gondwana (Argentina, 26°-29°S). Journal of Metamorphic Geology 21, 649-662.
Lucassen, F., Becchio, R., Wilke, H.G., Thirwall, M.F., Viramonte, J., Franz, G., Wemmer, K. 2000. Proterozoic-Paleozoic development of the basement of the Central Andes (18°-

26°)- a mobile belt of the South American craton. Journal of South American Earth Science 13, 697-715.

Lucassen, F., Franz, G., 2005. The early Paleozoic Orogen in the Central Andes: a non-collisional orogen compatible to the Cenozoic high plateau? In: Vaughan, A.P.M., Leat, P.T., Pankhurst, R.J. (Eds.), Terrane processes at the margins of Gondwana. Geological Society, London, Special Publications 246, pp. 257-273.

Ludwig, K.R., 1999. Isoplot/Ex Version 2.06. Berkeley Geochronology Center. Special Publications No. 1a, Berkeley, California.

Müller, W., Dallmeyer, R.D., Neubauer, F., Thöni, M., 1999.Deformation-induced resetting of Rb/Sr and 40Ar/39Ar mineral systems in a low-grade, polymetamorphic terrane (eastern Alps, Austria). Journal of the Geological Society, London, 156, 261-278.

Omarini, R.H., Sureda, R.J., Götze, H.J., Seilacher, A., Pflüger, F., 1999. Puncoviscana folded belt in northwestern Argentina: testimony of Late Proterozoic Rodinia fragmentation and pre-Gondwana collisional episodes. International Journal of Earth Sciences 88, 76-97.

Omarini, R., Viramonte, G., Cordani, U., Salfity, J.; Kawashita, K., 1984. Estudio geocronológico Rb-Sr de la Faja Eruptive de la Puna en el sector de San Antonio de los Cobres, Provincia de Salta, Argentina. Actas IX Congreso Geológico Argentino, San Carlos de Bariloche 3, 146-158.

Ramos, V. 1999. Rasgos estructurales del territorio argentino. 1. Evolución tectónica de la Argentina. In: Caminos, R. (Ed.), Geología Argentina. Segemar. Instituto de Geología y Recursos Minerales, Anales 29 (24), 715-784.

Ramsay, J.G., Graham, R.H., 1970. Strain variation in shear belts. Canadian Journal of Earth Sciences 7, 768 – 813.

Ramsay, J.G., Huber, M. I., 1983. The Techniques of Modern Structural Geology. Strain Analysis. Academic Press.

Rapela, C.W., Coira, B., Toselli, A., Saavedra, J., 1992. The Lower Paleozoic magmatism of southwestern Gondwana and the evolution of the Famatinian orogen. International Geology Review 34, 1081-1142.

Riller, U., Schwerdtner, W. M., 1997. Midcrustal deformation at the southern flank of the Sudbury Basin, central Ontario. Geological Society of America Bulletin 109, 841-854.

Riller, U., Oncken, O., 2003. Growth of the central Andean Plateau by tectonic segmentation is controlled by the gradient in crustal shortening. Journal of Geology 111, 367-384.

Rossi, J.N., Toselli, A.J., Durand, F.R., 1992. Metamorfismo de baja presión, su relación con el desarrollo de la cuenca Puncoviscana, plutonismo y régimen tectónico. Argentina. Estudios Geológicos 48, 279-287.

Schwerdtner, W.M., 1998. Graphic derivation of the local sense of shear strain components in the stretched walls of lithotectonic boundaries. Journal of Structural Geology 20, 957-967.

Schwerdtner, W.M., Riller, U., Borowik, A., 2005. Structural testing of tectonic hypotheses by field-based analysis of distributed tangential shear: concrete examples from major high-strain zones in the Grenville Province and other parts of the southern Canadian Shield. Canadian Journal of Earth Sciences 42, 1905-1925.

Turner, J.C., 1960. Estratigrafía de la Sierra de Santa Victoria y adyacencias. Boletín de la Academia de Ciencias de Córdoba 41, 163-196.

Villa I.M., 1998. Isotopic closure. Terra Nova 10, 42-47.

Viramonte, J.M., Becchio, R.A., Viramonte, J.G., Pimentel, M.M., Martino, R.D., 2007. Ordovician igneous and metamorphic units in southeastern Puna: New U-Pb and Sm-Nd data and implications for the evolution of northwestern Argentina. Journal of South American Earth Sciences 24, 167-183.

Wintsch, R.P., Christofferson, R., Kronenberg, A.K., 1995. Fluid-rock reaction weakening of fault zones. Journal of Geophysical Research 100, 13021-13032.

Zimmermann, U., Bahlburg, H., 2003. Provenance analysis and tectonic setting of the Ordovician clastic deposits in the southern Puna basin, NW Argentina. Sedimentology 50, 1079-1104.

Tables

Table 1. Fabric quantities used in Figure 8.

Station	SFI	LTB	S	L (x-axis)	z-axis	y-axis	LTB'	LTBn'	γx	γz	γx'	γn'
36	I	225/75	260/54	270/40	080/36	174/04	225/26	045/54	288/62	150/40	165/21	281/16
34	II	225/75	253/64	271/60	073/26	173/08	225/28	045/62	280/66	146/30	265/26	271/23
29	III	225/75	280/46	279/45	100/44	010/02	225/60	045/40	298/52	150/40	282/44	158/32
31	III	225/75	250/60	280/52	070/30	170/16	225/45	045/45	290/59	148/40	263/30	290/20
123	IV	225/75	240/60	235/50	060/30	328/04	225/48	045/42	256/73	153/48	240/45	280/32

SFI is visually estimated shape fabric intensity

Table 1: Fabric quantities used in Figure 8.

Table 2. Rb-Sr data of white mica (wm) and K-feldspar (kfs) displayed in Figure 9.

Sample	Sr [ppm]	Rb [ppm]	$^{87}Rb/^{86}Sr$	$^{87}Sr/^{86}Sr$	$^{87}Sr/^{86}Sr$ $2\sigma_m$ [%]
Pegmatitic dike MW 00-281: 455.8 ± 3.6 Ma *(n = 5, MSWD = 1.4)*					
fsp I-a	27.1	1.63	0.174	0.721829	0.0012
fsp I-b	21.1	5.48	0.753	0.725552	0.0016
wm 1	2.71	1021	3580	24.0398	0.0048
wm 2	3.21	1072	2480	16.6773	0.0082
wm 3	1.89	989	52000	341.465	0.0224
Mylonite MW 00-137b: 437.0 ± 3.8 Ma *(n = 5, MSWD = 1.12)*					
kfs < 160 µm	150	112	2.17	0.732293	0.0012
kfs > 0.5 mm	214	244	3.30	0.739333	0.0012
wm 250-160 µm	23.3	404	51.7	1.03961	0.0026
wm 355-250 µm	15.9	436	83.4	1.23378	0.0018
wm 500-355 µm	12.9	422	101	1.35493	0.0016
Mylonite MW 00-151: 436 ± 20 Ma *(n = 6, MSWD = 7.2)*					
428.4 ±4.5 Ma *(using wm250-160 µm, wm 160-100 µm, kfs < 160 µm)*					
kfs >0.5 mm	125	331	7.71	0.761277	0.0018
kfs <160 µm	72.0	180	7.27	0.759457	0.0012
wm 500-355 µm	7.13	653	317	2.74249	0.0038
wm 355-250 µm	8.02	628	263	2.33867	0.0014
wm 250-160 µm	7.29	650	305	2.57850	0.0014
wm 160-100 µm	7.16	642	307	2.58889	0.0018

Errors reported at 2σ level. An uncertainty of 1.5 % is assigned to Rb/Sr ratios.

Figure captions

Figure 1: (a) Simplified geological map showing exposure of Paleozoic rocks in NW-Argentina. (b) Close-up of (a) showing the greater Cerro Durazno area as well as the trend of prominent ductile deformation zones.

Figure 2: Simplified geological map showing Cenozoic faults, exposure of Paleozoic granitoid plutons and their crystallisation ages. Methods used to determine the crystallisation ages of minerals are as follows: (1) U-Pb monazite (Lork et al., 1989; Lork and Bahlburg, 1993), (2) U-Pb monazite and titanite (Büttner et al., 2005), (3) Rb-Sr whole rock (García and Rossello, 1984), (4) U-Pb monazite (Omarini et al., 1984), (5) U-Pb zircon (Haschke et al., 2005), (6) U-Pb zircon (Viramonte et al., 2007).

Figure 3: Geological map of the Cerro Durazno Pluton and its host rocks. Barbs in the Agua Rosada Shear Zone point towards the dip direction of planar metamorphic mineral fabrics. Sampling locations for Rb-Sr analysis of the pegmatite (MW00-281) and mylonite (MW00-137b and MW00-151) are shown in bold letters. Stippled lines delineate zones of metamorphic mineral shape fabric intensities, the levels of which are labelled with Roman numbers. Symbols denoting intensity of enclave shapes and d-values (Ramsay and Huber, 1983) correspond to those in Figure 5.

Figure 4: Mineral shape fabrics of the Cerro Durazno Pluton and its host rocks. (a) Metamorphic mineral lineations and strike trajectories of inclined planar shape fabrics. Dip magnitudes are mean values of a given area. Diagrams are lower-hemisphere equal-area projections of (b) poles to magmatic layering, (c) poles to metamorphic layering, (d) metamorphic mineral lineations of the entire area and (e) metamorphic mineral lineations of the Agua Rosada Shear Zone.

Figure 5: Modified Flinn-diagram (Flinn, 1962). R_{ab} is the average ratio of the maximum and intermediate diameters and R_{bc} the ratio of the intermediate to minimum diameters of enclave ellipticity. The symbols correspond to those used in the legend of Figure 3.

Figure 6: Determination of the direction of the shear strain γ on a lithotectonic boundary (LTB) with normal n, using a hypothetical L-S shape fabric after Schwerdtner (1998). The lineation direction (L) is parallel to the x-axis, and the z-axis is normal to foliation plane (S). The smaller the angle between γx and γz, the closer is the approximation of the γ direction. (a) Schematic block diagram depicting the geometric relationship between fabric quantities. (b) Graphical derivation of the possible range of shear strain directions in a lower-hemisphere equal-area projection. (c) The shear strain γ lies in the acute angle defined by γx and γz on the LTB.

Figure 7: Graphical derivation of shear strain γ for the Agua Rosada Shear Zone for the two kinematic scenarios. (a) Lithotectonic boundary (LTB) is steeper than S and (c) lithotectonic boundary (LTB') is shallower than S. The possible ranges of shear strain γ on LTB and LTB' is indicated by thick lines with arrowheads on both ends. (b) and (d) are respectively schematic NE-SW profiles of scenario (a) and scenario (b). Explanation of both scenarios as well as fabric and shear strain parameters is given in the text.

Figure 8: Geological map showing zones of equal shape fabric intensity in the Cerro Durazno Pluton and the Agua Rosada Shear Zone. Lower-hemisphere equal-area projections display possible shear strain directions for variable orientations of lithotectonic boundaries, LTB and LTB', for five areas. The kinematics of deformation is delineated in the text. Fabric and shear strain parameters used are given in Table 1.

Figure 9: Rb-Sr isochron diagrams of (a) an undeformed pegmatite (MW00-281), (b) Agua Rosada mylonite (MW00-137b) and (c) Agua Rosada mylonite (MW00-151). See Table 2 for analytical results.

Figures

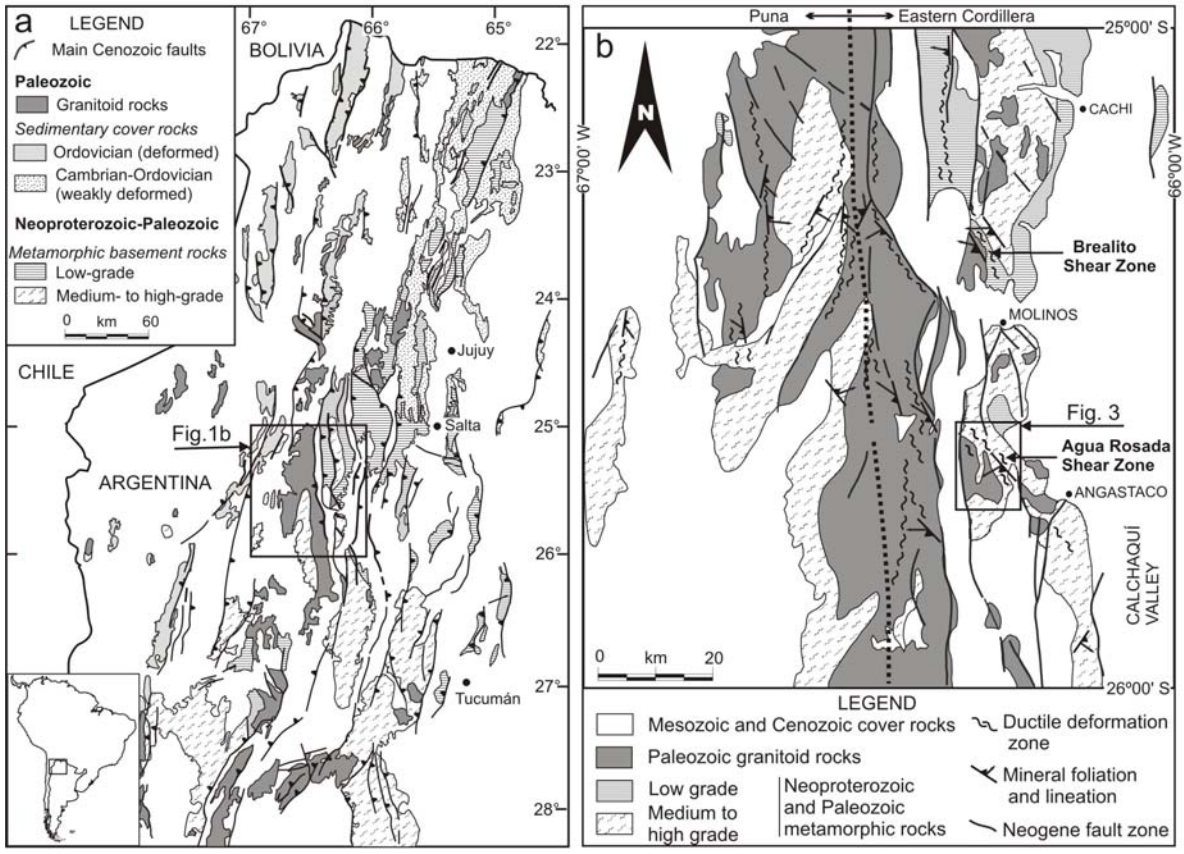

Wegmann et al. Figure 1

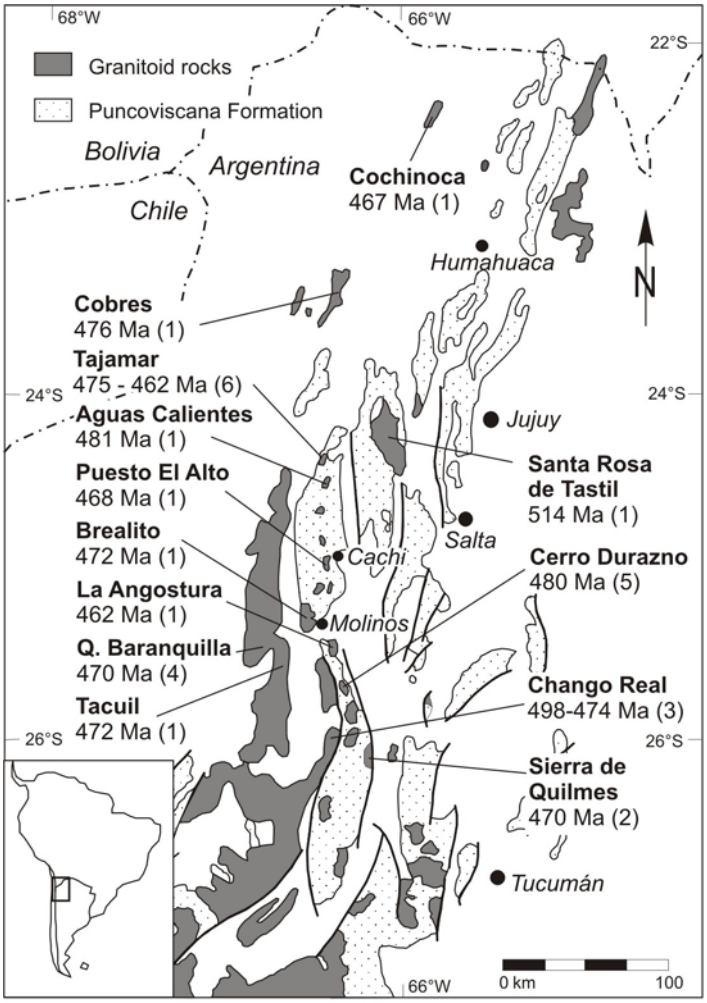

Wegmann et al. Figure 2

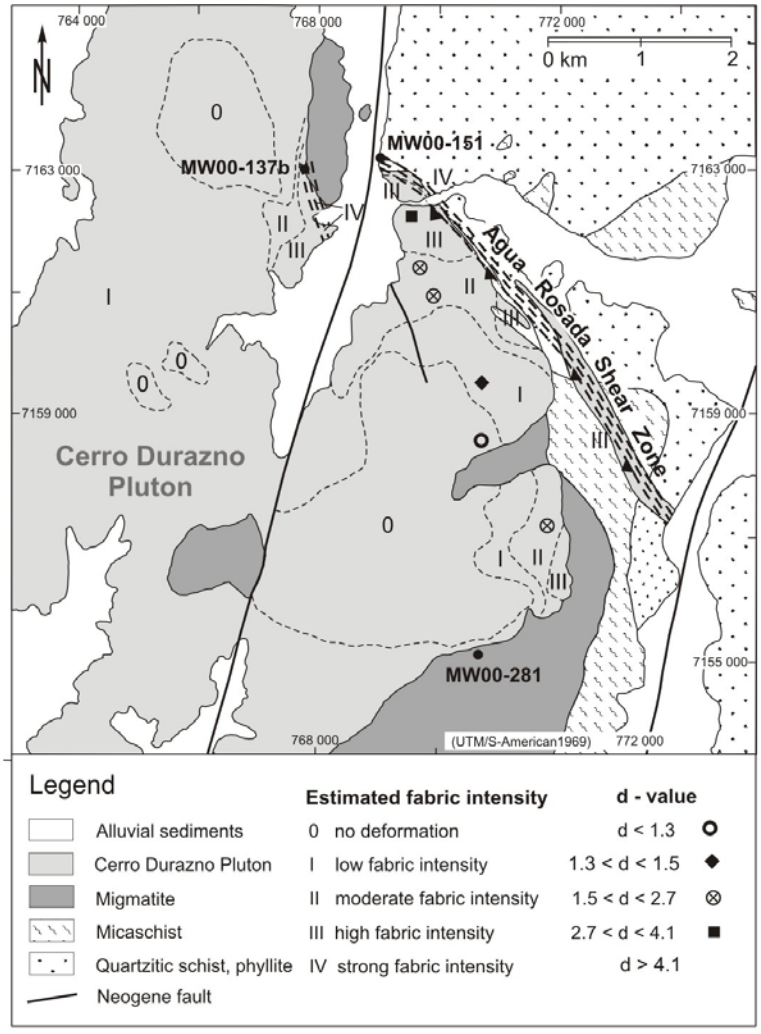

Wegmann et al. Figure 3

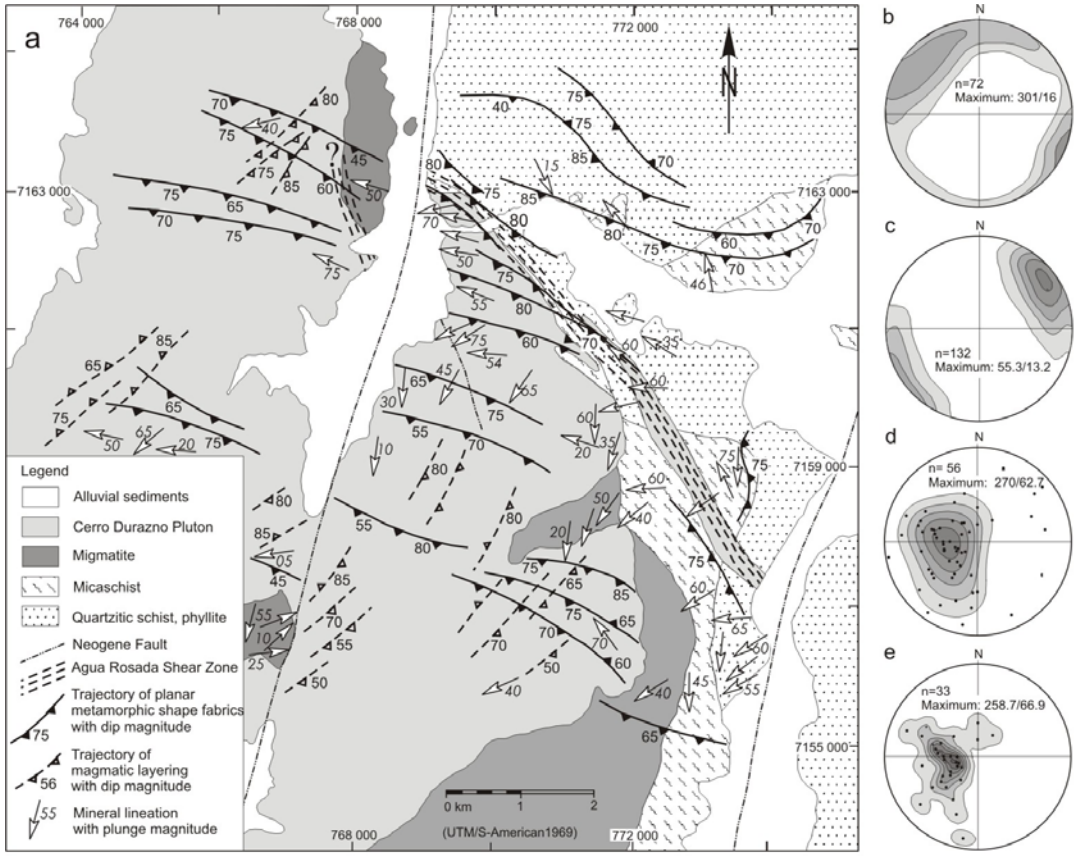

Wegmann et al. Figure 4

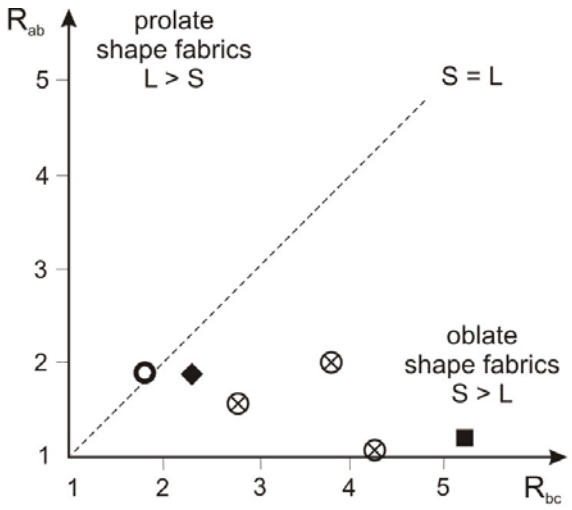

Wegmann et al. Figure 5

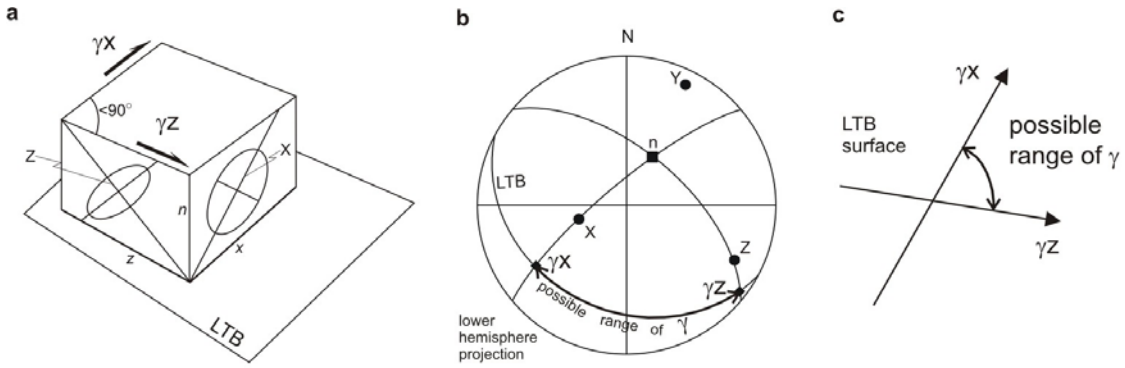

Wegmann et al. Figure 6

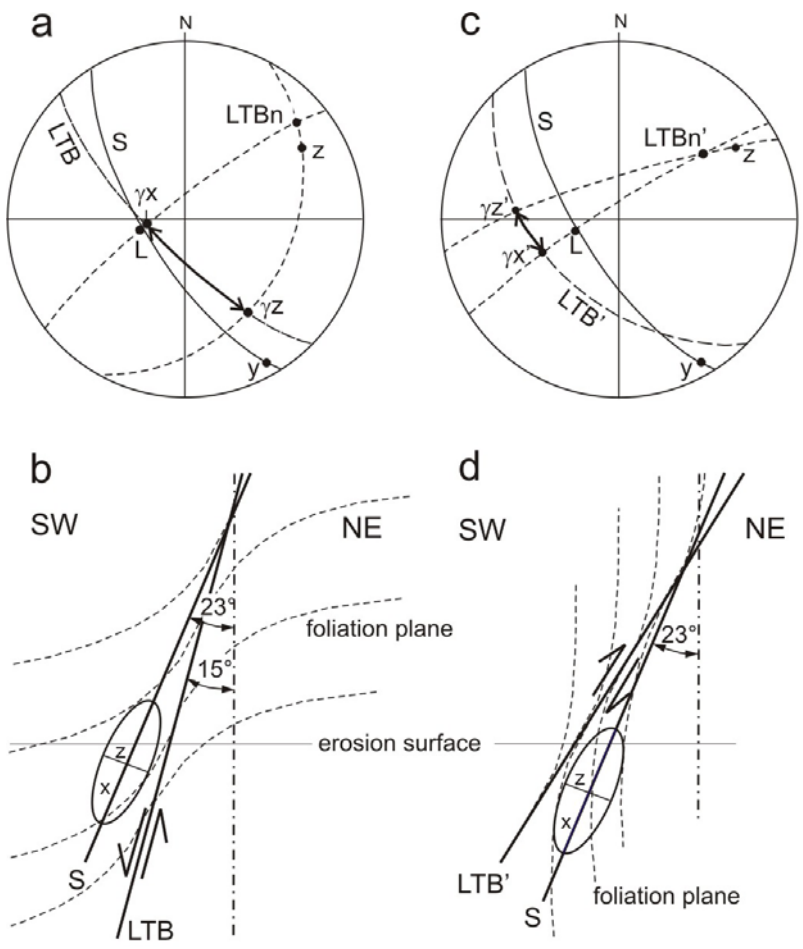

Wegmann et al. Figure 7

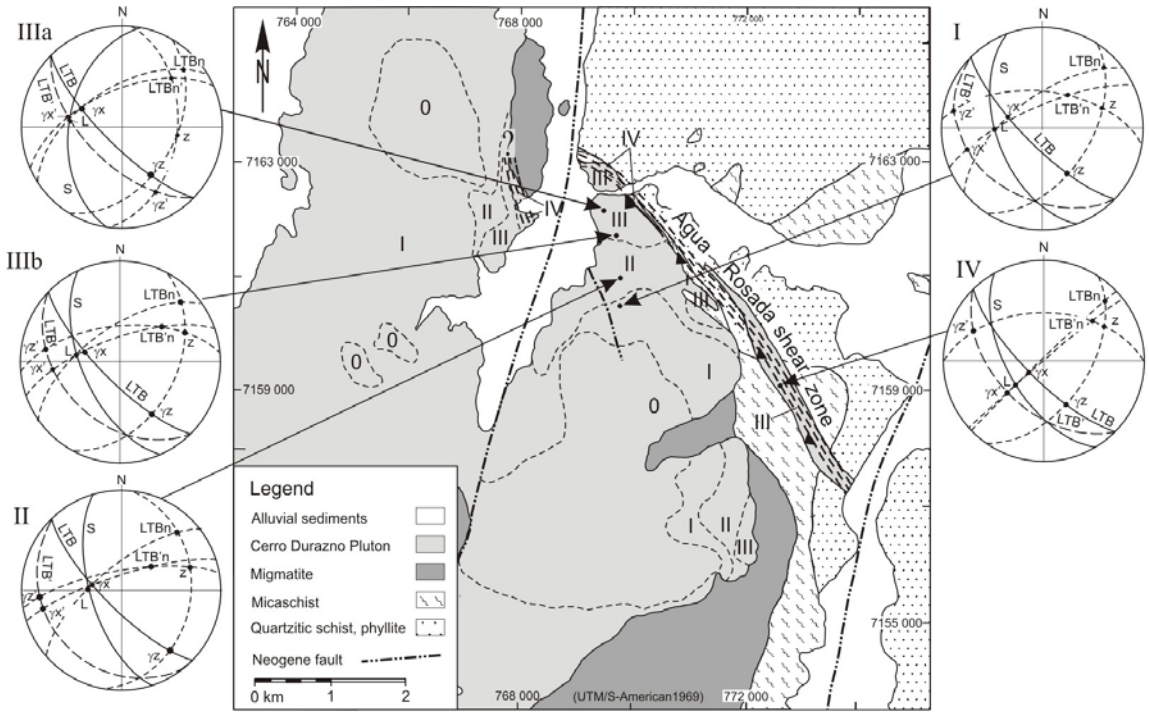

Wegmann et al. Figure 8

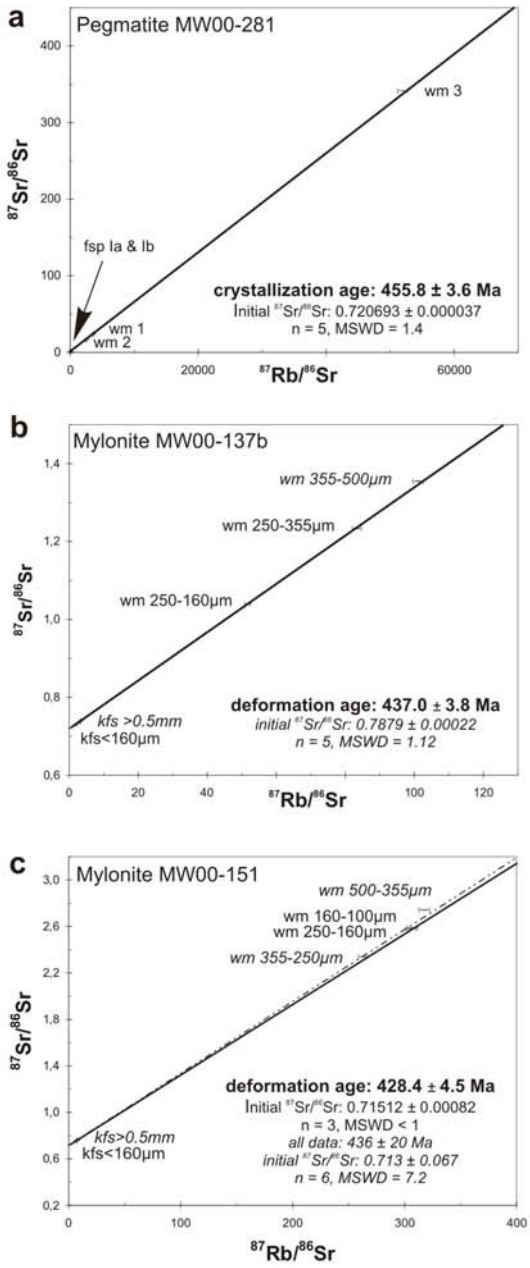

Wegmann et al. Figure 9